RSC Advances

Photocatalytic Properties of Polydopamine-Modified Ag NPs/TiO2 Porous nanofibers prepared by Electrospinning

Journal:	*RSC Advances*
Manuscript ID	RA-ART-08-2015-016797.R2
Article Type:	Paper
Date Submitted by the Author:	13-Nov-2015
Complete List of Authors:	Wang, Huaiyuan; Northeast Petroleum University, College of Chemistry and Chemical Engineering Jiang, Feng; Northeast Petroleum University, College of Chemistry and Chemical Engineering Zhu, Yanji; Northeast Petroleum University, College of Chemistry and Chemical Engineering Zhao, Ya'nan; Northeast Petroleum University, College of Chemistry and Chemical Engineering
Subject area & keyword:	Photocatalysis < Catalysis

Photocatalytic Properties of Polydopamine-Modified Ag NPs/TiO_2 Porous nanofibers prepared by Electrospinning

Huaiyuan Wang*, Feng Jiang, Yanji Zhu, Ya'nan Zhao

College of Chemistry and Chemical Engineering, Northeast Petroleum University, Daqing 163318, Heilongjiang Province, People's Republic of China

Abstract: Polydopamine-modified Ag/TiO_2 porous nanofibers (PDA-Ag/TiO_2 porous NFs) bionic composite catalysis was successfully prepared via a simple electrospinning process combined with impregnation method. It was found that the PDA-Ag/TiO_2 porous NFs present a corn-like, coarse, porous structure when the TiO_2 NFs look like corn cod and the Ag nanoparticles (NPs) act as corn kernels. In our research, carbon nanotubes (CNTs) were embedded in the original spinning as the pore former by electrospinning. After calcination, the loss of the CNTs left a lot of holes in the internal of the TiO_2 NFs that make the specific surface area increasing about 30 percent compared to the pure TiO_2 NFs. Ag NPs embedded in the TiO_2 NFs could prevent the recombination of electron-hole pairs generated from photocatalysis and transfer the captured electron to participate the reaction of photocatalysis process. The PDA which wrapped TiO_2 NFs homogeneously could adsorb the organic matter and promote the spatial separation of photogenerated charges. The higher photocatalysis efficiency demonstrated a synergy between the Ag NPs and PDA with PDA played the role of the gripper to capture organic molecules, and the Ag NPs

* Corresponding author. Tel: +86 4596503083; fax: +86 4596503083.
E-mail address: wanghyjiji@163.com

dopped in the TiO_2 NFs as the electron conveyer which could refrain the recombination of electron-hole pairs. The new bionic composite catalyst has potential application for cleaning up organic pollutants.

Key Words: PDA-Ag/TiO_2 nanofibers; Porous; Electrospinning; Photocatalysis; Synergy.

1.Introduction

With the rapid pace of the development of economy and technology, environmental pollution has become the major global issue to all beings. Water is the most important resource of human beings. However, the reckless discharge of untreated industrial wastewater contains organic and inorganic contaminant that pollutes the natural water bodies in recent years. The water pollution problem has become an urgent issue which requires immediate solution [1, 2].

Titanium dioxide has aroused widely research interests because of its versatility and potential applications in the fields of science and technology [3-5]. As the continuous pollution of the water resources, titanium dioxide has obtained a profound study in the field of sewage treatment for its nontoxicity, recyclability and affordability [6, 7]. Dyestuff, saccharides, and oils in wastewater could be mineralized to achromatous and innoxious inorganic small molecules after photocatalytic reaction by titanium dioxide [8]. However, titanium dioxide has some disadvantages which limit its practical application, such as recombination of photo-generated electron-hole pairs, high band gap and low efficiency of quantum in photocatalytic activity [9-10].

In recent years, several methods have been devoted to modify the surface of titanium dioxide to improve its photocatalysis efficiency. The metal/TiO_2 composites attract many researchers due to its efficient optical/electronic performance and bifunctional characteristic [11]. Silver modified TiO_2 have been studied to the degradation of dyes and showed superior performance [12].

More recently, dopamine has caught a wide range of interest due to its unique properties. Dopamine, a mussel-inspired protein, has revealed remarkable performance [13-19] such as biosensor [13], catalysis [14], and energy storage [15] . Some groups have found out that dopamine modified titanium dioxide enables utilizing of visible light and promote the separation of electrons and holes [20]. What is more, due to super-adhesion capability of dopamine, some scientists found that it could self-polymerize to polydopamine (PDA) and deposit on the surface of organic and inorganic matter effectively [21-23].

In this paper, a simple and effective method to produce PDA-Ag/TiO_2 porous NFs bionic composite catalysis is illustrated. Our approach consists of several technical advantages including simple pore-forming method with CNTs to increase its specific surface area, easy fabrication of Ag NPs onto TiO_2 NFs without the step of further deposition and a feasible way to modify a shallow but efficient PDA layer.

2. Experimental

2.1 Materials

Polyvinyl Pyrrolidone (PVP, average 1300000 MW) Hangzhou Lvke Technology Co., Ltd(China), silver nitrate ($AgNO_3$, AR, 99.5%) were purchased from Shanghai Shiyi Chemical Reagent Co., Ltd (China). Tetrabutyl titanate (Ti $(OC_4H_9)_4$, CP, 98.0%) was obtained from Tianjin Fuchen Chemical Reagent Factory (China). Ethanol (C_2H_5OH, AR, 99.7%) and acetic acid (CH_3COOH, AR, 99.5%) were provided by Shenyang Huadong Chemical Reagent Factory (China). Dopamine and tris (hydroxymethyl) aminomethane hydrochloride (Tris-HCl) were supplied from Suzhou

Tianke Trade Co.,Ltd. The CNTs (diameter: 20-40 nm) were provided by Nanjing XF Nano Materials Tech Co., Ltd. All aqueous solutions were prepared with high purity water (>18.3 MΩ-cm) by a Millipore Milli-Q system at 25 ^{o}C.

2.2 Preparation of Ag NPs/TiO_2 precursor electrospinning solutions

0.02 g $AgNO_3$ was thoroughly dissolved in 9.8 g ethanol at room temperature under continuous stirring in the dark environment for 1 hour. Then, 1.0 g PVP powder was added and stirred for 12 hours avoiding the light. Subsequently, 6 drops of acetic acid, 4.8 g $Ti(OC_4H_9)_4$ and 1.0 g CNTs were added into the acquired brown colored solution followed by stirred for 5 hours to form electrospinning precursor solution.

2.3 Synthesis of Ag/TiO_2 porous NFs

The electrospinning equipment principally consists of four parts, a high voltage power supply, a plastic syringe with a stainless steel needle (the inner diameter was 1 mm), micro-injection pump, and a rotary collector. Firstly, the electropinning precursor solution was immediately loaded into the plastic syringe, the syringe then intalled to the micro-injection pump and the distance between the needle tip and the rotary collector was 13 cm. The high-voltage power supply is connected to the needle with a copper split pin and the voltage setting at 20 kV. All of the experiments were performed under the condition of air atmosphere and room temperature. After electrospinning, prepared mat of the composite NFs were dried at 60 ^{o}C for 12 hours at a drying oven and then calcined in air atmosphere at 550 ^{o}C for 3 hours with a heating rate of 3 ^{o}C/min.

2.4 Preparation of PDA-Ag/TiO_2 porous NFs

The NFs obtained after calcination were infused in a mixture of dopamine, tris and distilled water for 120min (TiO_2: tris: dopamine: water=0.3: 0.0243: 0.002: 50; m/m/m/m). Subsequently, the NFs washed with distilled water three times and then dried in the drying oven at 60 ^oC for 8 hours.

2.5 Preparation of pure TiO_2 NFs and porous TiO_2 NFs

Two blank samples of pure TiO_2 NFs and porous TiO_2 NFs were prepared by electrospinning. Firstly, 1.0 g PVP polymer was added to 9.8 g ethanol and stirred for 12 hours at room temperature. 10 drops of acetic acid, 4.8 g $Ti(OC_4H_9)_4$ were added and stirred for 5 hours to form electropinning precursor solution. With the electrospinning conditions of 20 kV voltage and the nozzle to a collector at the distance of 13 cm, the prepared nanofibers were calcined in air atmosphere at 550 ^oC for 3 hours with a heating rate of 3 ^oC/min after dried. The obtained NFs were the pure TiO_2. The other samples of porous TiO_2 NFs were prepared by the same way besides the precursor solution was added 0.1 g CNTs to pore-forming.

2.6 Photocatalytic tests

The equipment used for photocatalytic test mainly consists of four parts, a quartz reactor (the diameter was 50 mm, the capacity was 100 mL), the ultraviolet lamp (175 W) placed above the reactor about 15 cm was purchased from Beijing Trusttech Co. Ltd., China, a magnetic stirrer and the cooling equipment. The photocatalytic activity of pure TiO_2 NFs, porous TiO_2 NFs, Ag/TiO_2 porous NFs and PDA-Ag/TiO_2 porous NFs were measured by photocatalytic degradation of methyl orange. Methyl orange aqueous solution (20 mg/L, 100 mL) and nanofibers (25 mg) was magnetically

stirred in a dark environment for 30 minutes to reach adsorption-desorption equilibrium between the organic molecules and the catalyst surface. The acidity of the solution was neutral. Subsequently, the ultraviolet light was turned on and the photocatalytic degradation reaction was proceeding. The whole system was open to air and the reaction temperature of the suspension was maintained at 303 K by circulation of water through cooling equipment. During the irradiation, 5 mL reaction solution was taken out to be used for analysis every 10 minutes.

2.7 Photocatalytic Evaluation

The reaction solution obtained from photocatalytic tests was centrifuged and filtrated. The filtrates were analyzed with a UV-vis-NIR scanning spectrophotometer at 554 nm.

2.8 Characterization

The morphology of the nanofibers was detected by scanning electron microscope (SEM, Quanta 200, China) and transmission electron microscope (TEM, JEM-1010, Japan). Brunner−Emmet−Teller (BET) data were acquired using a specific surface area instrument (TristarII 3020M, America). The chemical composition of the prepared NFs was scrutinized by infrared spectrometer (FT-IR, Tensor27, China) and X-ray diffraction (XRD, D/max2200, Japan). UV–visible spectroscopy was performed with UV-vis-NIR scanning spectrophotometer (UV3150, China).

3 Results and discussion

3.1 Preparation process

According to the experimental procedures, the preparation and synthesis mechanism of PDA-Ag/TiO_2 porous NFs are illustrated in Scheme 1. Firstly, TiO_2/PVP/$AgNO_3$/CNTs composite NFs were produced by electrospinning process (shown in Scheme 1a). After completed hydrolyzation and calcination at 550 ^oC for 3 h in a muffle, PVP and CNTs were removed completely and remained porous NFs with many internal holes (Scheme 1b). Then the Ag/TiO_2 porous NFs were transferred into the solution involved tris and dopamine. By the polymerization of dopamine, the PDA layer was deposited on the TiO_2. After cleaning and drying, the black color PDA layer was clearly observed to be coated on the surface of TiO_2 NFs homogeneously (shown in Scheme 1c).

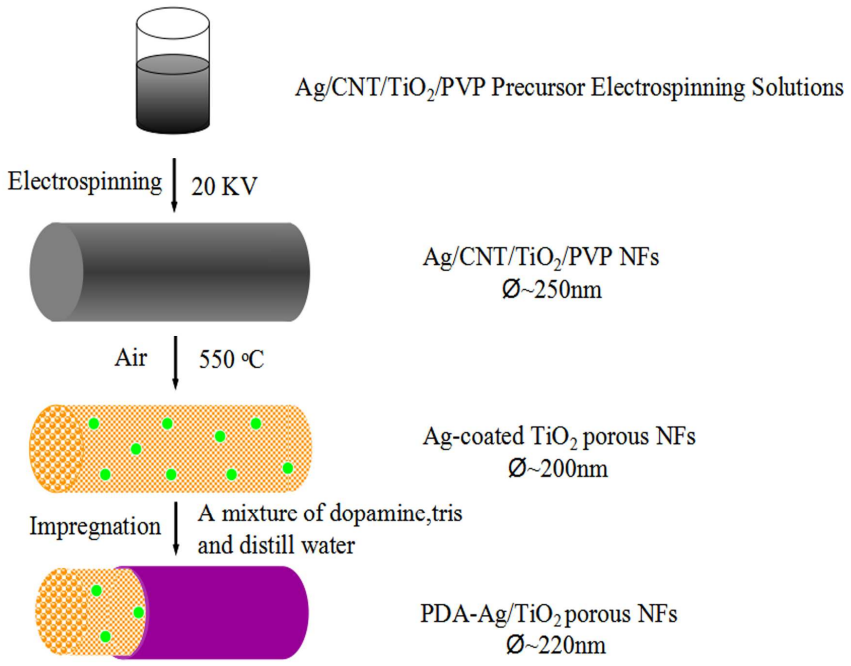

Scheme 1. Illustration of synthesis of dopamine-modified Ag/TiO_2 porous NFs

3.2 SEM of the samples

SEM images are used to confirm the morphology and diameter size of the resulting materials. Fig. 1a shows a typical image of the pure TiO_2 electrospun NFs with an average diameter of 200 nm, the surface is uniform and smooth as shown in the Fig. 1a. The porous TiO_2 NFs are observed to remain continuous fibrous structures with the average diameter of 200 nm, but the surface is rough and porous as shown in Fig. 1b. As shown in Fig.1c, there exists a small quantity of the Ag NPs distributed evenly throughout the surface of TiO_2 NFs. The size of the Ag NPs distributes range from 6 nm to 20 nm. Fig.1d shows SEM images of the PDA-Ag/TiO_2 porous NFs. The surface of the PDA-Ag/TiO_2 porous NFs is much smoother than the TiO_2 porous NFs and the Ag/TiO_2 porous NFs as shown in Fig. 1b and Fig. 1c. The morphology of the PDA film can't be seen clearly in Fig.1d. Therefore, the TEM images of the PDA-Ag/TiO_2 porous NFs are provided in Fig.2.

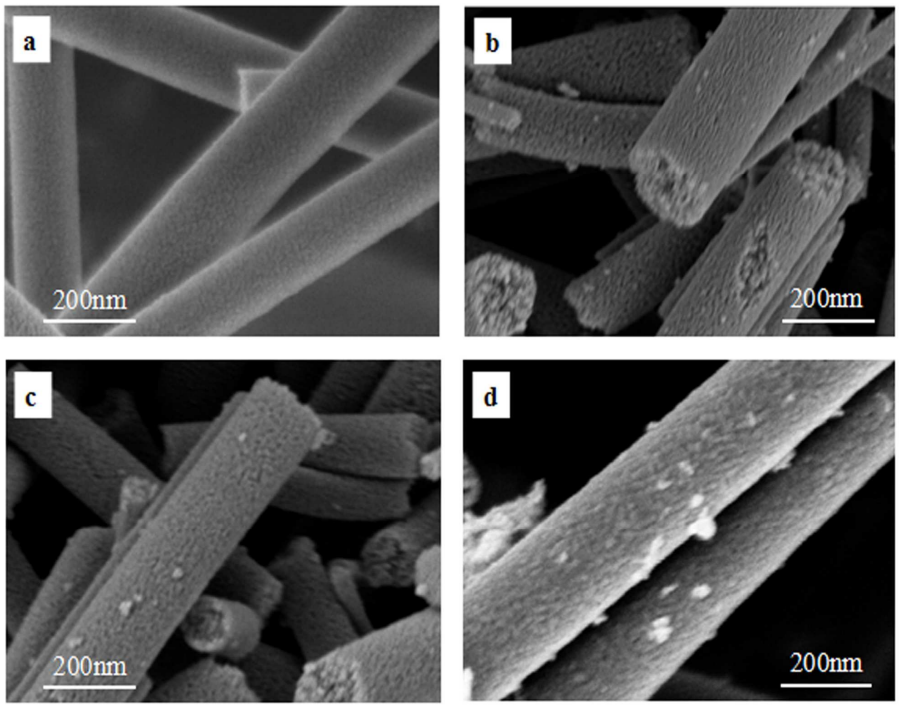

Fig. 1. SEM images of (a) pure TiO_2 NFs, (b) porous TiO_2 NFs, (c) Ag-TiO_2 porous NFs, (d) PDA-Ag/TiO_2 porous NFs.

3.3 TEM of the PDA-Ag/TiO_2 porous NFs

In order to prove the PDA film was compact and uniform on the surface of TiO_2 NFs, TEM images of PDA-Ag/TiO_2 NFs is shown in Fig.2. As shown in Fig.2a, we could clearly see some small Ag NPs encapsulate in the TiO_2 NFs. The size of Ag NPs is centered at 10 nm. At the edge of the TiO_2 NFs, the PDA film which wraps the TiO_2 NFs homogeneously is clearly seen. Fig. 2b is the larger magnification of Fig. 2a. The approximate thickness of the PDA film was about 5-10 nm.

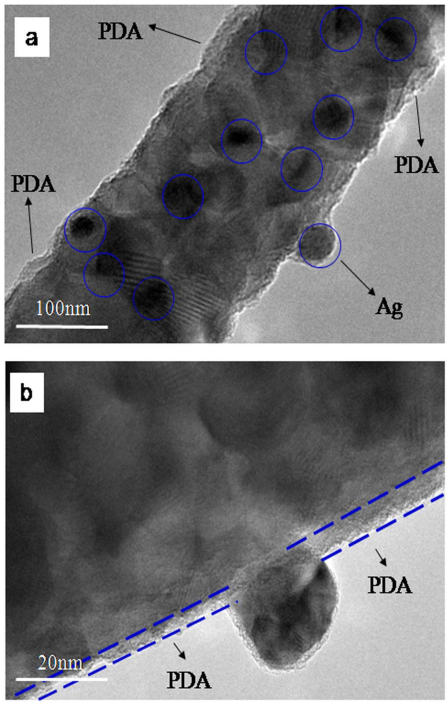

Fig. 2. TEM images of (a) PDA-Ag/TiO2 porous NFs and (b) larger magnification of it.

3.4 XRD patterns

XRD patterns of the pure TiO_2 (3a) NFs, porous TiO_2 (3b) NFs, Ag/TiO_2 porous NFs(3c), PDA-Ag/TiO_2 porous NFs (3d) are shown in Fig. 3. As seen, the spectra of

four samples all present the diffraction peaks at 2θ values of 25.37°, 37.03°, 37.86°, 38.61°, 48.12°, 53.97°, 55.10°, 62.14°, 62.74°, 68.79° and 75.0°, which indicate the formation of anatase phase (JCPDS files no. 21-1272). As shown in Fig. 3c-d, there are seven new diffraction peaks appear at 2θ values of 27.48°, 37.8°, 41.3°, 44.1°, 56.65°, 64.2° and 77.1°. The extra peaks which at 2θ values of 37.8°, 44.1°, 64.2° and 77.1° are matching the silver metal as we expected (JCPDS files no. 04-0783). The new absorption peaks are very weak because of the doping amounts of the Ag NPs are very small and highly dispersed. The peaks at 2θ values of 27.48°, 41.3°, 56.65° indicate the formation of the rutile titanium dioxide (JCPDS files no. 21-1276). The result proved that the addition of the silver could reduce the temperature of anatase phase change to rutile phase. Therefore, the Ag-dopped TiO_2 is more likely to form mixed crystal than pure TiO_2 which is one of the causes of the photocatalytic performance increasing. As shown in Fig. 3d, there are no new diffraction peaks been detected compared to Fig. 3c, it is because that there is no crystallization peak for PDA.

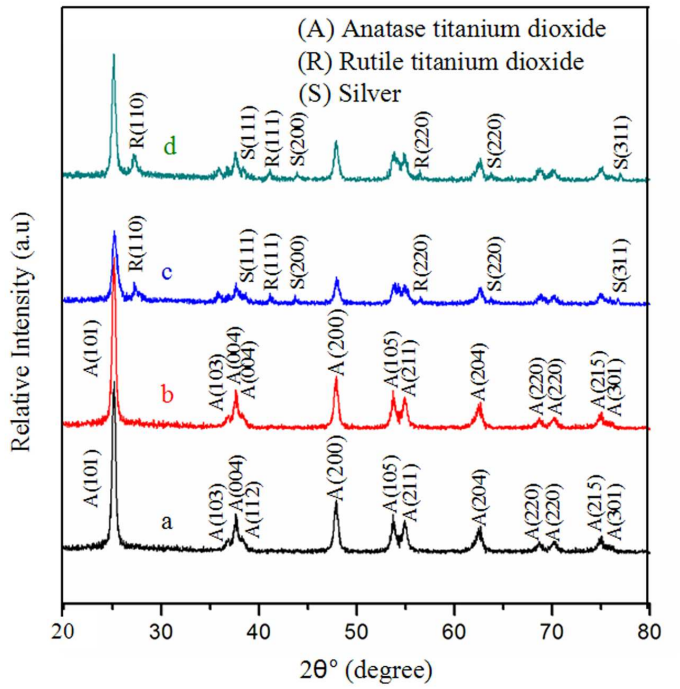

Fig. 3. XRD patterns of (a) pure TiO_2 NFs, (b) porous TiO_2 NFs, (c) Ag-TiO_2 porous NFs, (d) PDA-Ag/TiO_2 porous NFs

3.5 UV–visible absorption spectra

To test the optical absorption properties of the four samples, UV–visible spectroscopy was measured in the range of 300 to 800 nm. As shown in Fig. 4, pure TiO_2 (Fig. 4a, Fig. 4b) doesn't display any absorption capacity in the visible area. In Fig. 4c and Fig. 4d, the red shift was exhibited in both samples. It is easy to detect that there is a broadened peak at about 525nm in Fig.6c due to the Ag NPs doped into the lattice of TiO_2. It changes the electronic structure and improves the ability of the visible light response. In Fig. 4d, PDA-Ag/TiO_2 photocatalyst has higher absorption intensity compared with Ag/TiO_2 photocatalyst. This result demonstrated that PDA had photoresponse in the visible region.

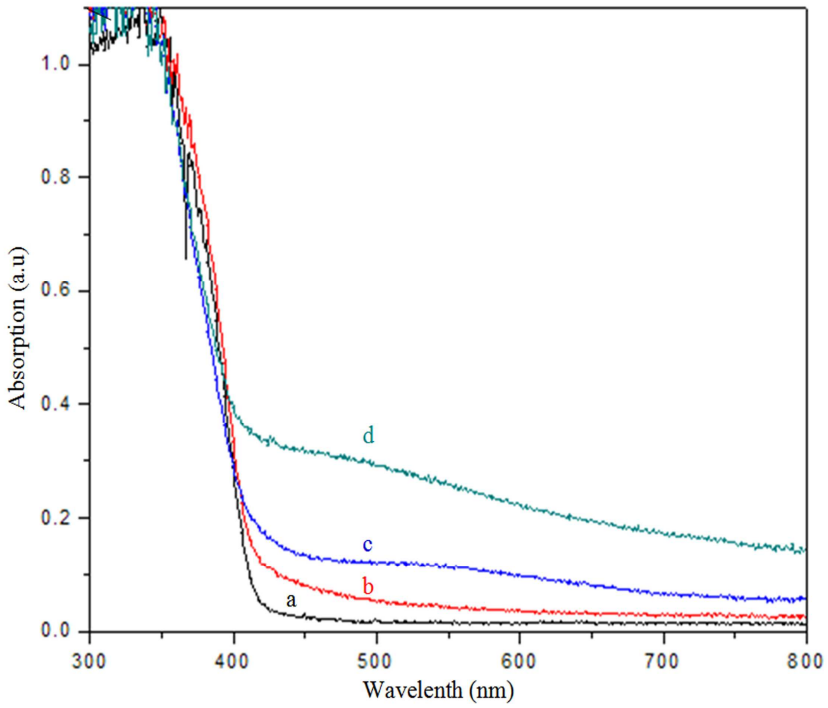

Fig. 4. UV–visible absorption spectra of (a) pure TiO_2 NFs, (b) porous TiO_2 NFs, (c) Ag/TiO_2 porous NFs, (d) PDA-Ag /TiO_2 porous NFs.

3.6 FT-IR spectra

The FT-IR spectra of pure TiO_2 and PDA-Ag/TiO_2 are shown in Fig. 5a. The band at 3422 cm^{-1} is associated with the stretching vibration of O-H, and the bands at 2922, 2851 and 1411 cm^{-1} can be attributed to the stretching vibration and bending vibration of C-H. The band observed at 1624 cm^{-1} is the characteristic peak of C=C. Compared with the FT-IR spectra of the pure TiO_2, the PDA-Ag/TiO_2 displays only one additional peak at 1457 cm^{-1} corresponding to the aromatic ring of PDA [24]. In addition, the peaks of O-H and saturation C-H become stronger, which is due to the introduction of PDA. In Fig. 5b, the FT-IR spectra of PDA-Ag/TiO_2 and the PDA-Ag/TiO_2 after 20 minutes photodegradation are shown. We could clearly notice that the spectrum of the

PDA-Ag/TiO_2 after reaction still has the characteristic peaks of PDA. It demonstrates that the PDA-Ag/TiO_2 still have the adsorption property after photocatalytic reaction. The adsorption reaction equation of PDA to methyl orange is shown in Fig. 5c.

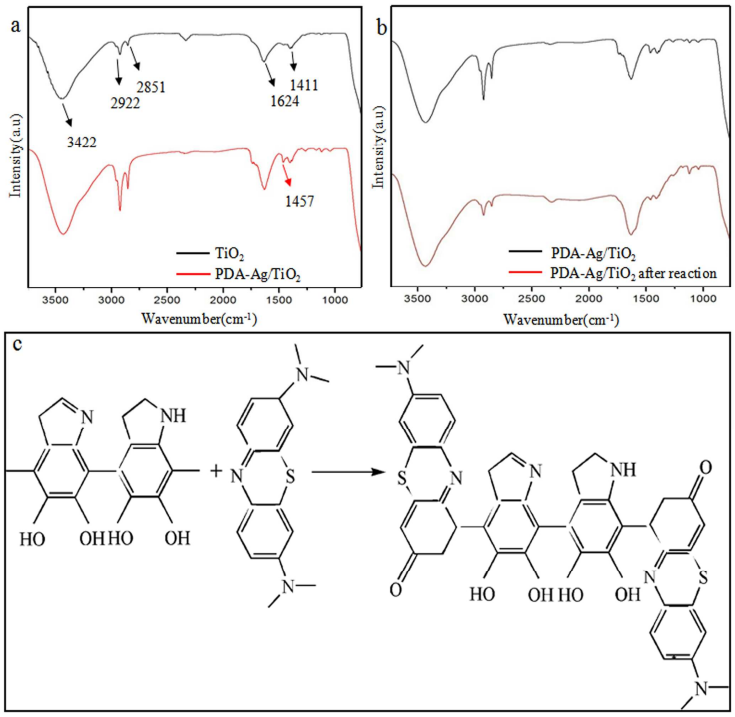

Fig. 5. (a) FT-IR spectra of the pure TiO2 and PDA-Ag/TiO2. (b) FT-IR spectra of the PDA-Ag/TiO2, and PDA-Ag/TiO2 after photocatalytic reaction. (c) The proposed adsorption mechanism between PDA and methyl orange.

3.6 Physicochemical characterization of the samples

Physicochemical characterization of the four photocatalysts was shown in Table 1. It indicates that porous TiO_2 photocatalyst has the highest BET surface area. This result is due to the porous channel structure increased by the disappearance of CNTs after calcination. The porous Ag/TiO_2 has lower BET surface area compares to the porous TiO_2. It is because that Ag NPs plugged some channels of the TiO_2 NFs. As

shown in Table 1, after the modification by PDA, the surface area increased from 32.2 m^2g^{-1} to 35.4 m^2g^{-1} own to the impregnation which made the secondary channel. There is no big change for the pore volume of the four photocatalysts. Experimentally, the four samples of TiO_2 NFs were used as photocatalysts in degradation of methyl orange under UV irradiation.

Table 1.

Physical characterization of four photocatalysts synthesized by electrospinning method.

Sample label	Color of the photocatalyst	S_{BET} (m^2g^{-1})	V_p (cm^3/g)
Pure TiO_2	White	29.9	0.07
Porous TiO_2	White	39.5	0.09
Porous Ag/TiO_2	Light gray	32.2	0.08
Porous PDA-Ag/TiO_2	Gray	35.4	0.09

3.7 Photocatalytic activity for degradation of methyl orange

The photocatalytic degradations of methyl orange were subsequently performed as a model reaction to evaluate the photocatalytic activities of the four samples under the simulated UV irradiation. As shown in Fig. 6a, after the stir of the catalysts in the methyl orange solution for 30 min in the dark condition, we could see the difference in the dye adsorption for the four samples. It is noteworthy that the adsorption activity of porous TiO_2 NFs was higher than that of the pure TiO_2 NFs, and the adsorption

activity of PDA-Ag/TiO_2 porous NFs was higher than that of the porous Ag/TiO_2 NFs. There is no big difference in the dye adsorption of porous TiO_2 NFs and Ag/TiO_2 porous NFs. After irradiation for 60 minutes, we can clearly found that the degradation activity of pure TiO_2, porous TiO_2, Ag/TiO_2 porous NFs and PDA-Ag/TiO_2 porous NFs were increasing gradually (pure TiO_2 < porous TiO_2 < porous Ag/TiO_2 < PDA-Ag/TiO_2). It could be found that only 40% and 55% of methyl orange molecules were degraded in 20 min for pure TiO_2 and porous TiO_2, respectively. By contrast, the degradation efficiency of methyl orange was about 70% and 85% after 20 min UV irradiation for Ag/TiO_2 porous NFs and PDA-Ag/TiO_2 porous NFs, respectively. As expected, PDA-Ag/TiO_2 porous NFs exhibited much more superior photocatalytic performance compared with pure TiO_2 nanofibers. As shown in Fig 6b and 6c, we could clearly find that the color of the dye solution contained PDA-Ag/TiO_2 porous NFs changed from orange to uncolored in the reaction process when solution with pure TiO_2 still had orange color 30 minutes later. This exciting result can be attributed to three reasons, (1) the high specific surface area of PDA-Ag/TiO_2 porous NFs, (2) Ag NPs dopped in the interior and surface of the TiO_2, (3) modification of TiO_2 NFs with PDA film.

Specific surface is an important factor which is affecting the photocatalytic performance. The high specific surface area means the high adsorption capacity, consequently, when the photocatalysts have the same degree of crystallinity, the higher the specific surface area of the photocatalyst, the better the photocatalytic

performance it will shows. This is the reason that the degradation activity of porous TiO_2 NFs was higher than the pure TiO_2 NFs.

It is well known the key factors of photocatalytic activity depend on several aspects, such as the photoelectron generation, the separation of electron-hole pairs, and the transfer efficiency of the electron. After Ag NPs doped the TiO_2 NFs, the photocatalytic performance was improved by two different types. On one side, Ag NPs could prevent the recombination of electron-hole pairs generated from photocatalytic reaction. On the other side, the Ag NPs also could transfer the captured electron to the adsorbed oxygen to participate in the reaction of photocatalysis process [26-28].

Modification of TiO_2 NFs with PDA could enhance the photocatalytic performance not only because PDA could adsorb the holes and promotes the spatial separation of photogenerated charges, but also the PDA (involving abundant -OH, -NH, -C=O, -S groups) just like a gripper which has high adsorption efficiency for organic matter.

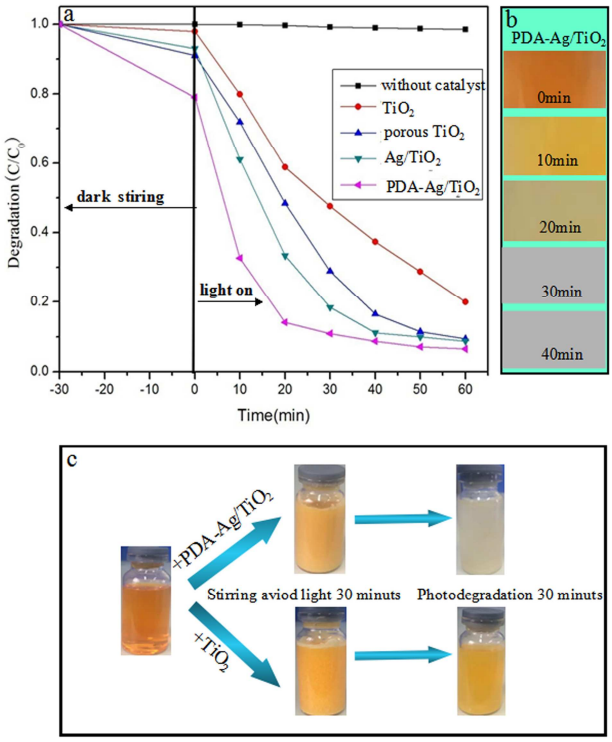

Fig. 6. (a) Photocatalytic degradation of methyl orange aqueous over different catalysts under ultraviolet light, (b) Photographs of methyl orange aqueous against irradiation time with the photocatalyst of PDA-Ag/TiO2, (c) Photographs of methyl orange aqueous following stirred avoid light for 30 min and after ultraviolet light irradiation of 30 min with the photocatalysts of PDA-Ag/TiO2 and pure TiO2.

3.8 Kinetic patterns

The kinetic pattern of degradation of methyl orange aqueous under the ultraviolet light irradiation of 20 min for the four samples is shown in Fig. 7. The rates manifest a very small dye decay rate under ultraviolet light illumination without any catalyst. The constant of reaction rates with the catalysts of pure TiO_2 NFs, porous TiO_2 nanofibers, Ag/TiO_2 porous NFs and $PDA\text{-}Ag/TiO_2$ porous NFs are $2.66\times10^{-2}\ min^{-1}$, $3.63\times10^{-2}\ min^{-1}$, $5.48\times10^{-2}\ min^{-1}$, $9.8\times10^{-2}\ min^{-1}$ respectively. This result indicates the $PDA\text{-}Ag/TiO_2$ porous NFs has the best superior photocatalytic performance with rate

constant of 9.8×10^{-2} min^{-1} which is nearly about four times than that of the pure TiO_2 NFs.

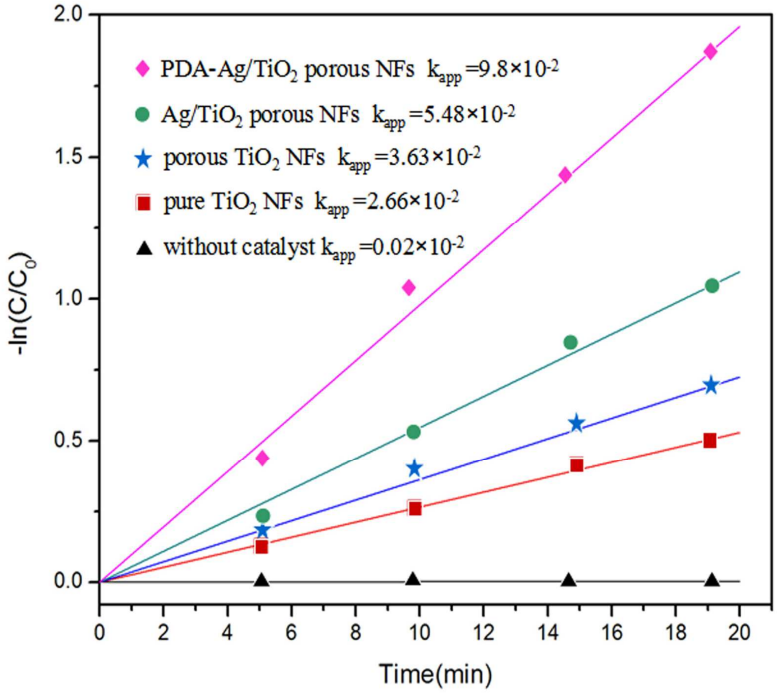

Fig. 7. Kinetics of methyl orange degradation in the 20 min under the ultraviolet light irradiation.

3.9 Mechanism for the photodegradation of methyl orange

The scheme in Fig. 8 illustrates the possible photocatalytic reaction involved in between PDA–Ag/TiO_2 and methyl orange molecules under UV irradiation. The Key features of the high photocatalytic efficiency are simplified to illustrate in this scheme. The key features include four aspects, the porosity of the composite, the independent action of Ag NPs and PDA, the synergistic action between Ag NPs and PDA. The porous structure of the PDA–Ag/TiO_2 bionic composite catalyst makes it adsorb more methyl orange molecules than the pure TiO_2 which increase the photocatalytic reaction faster. For the composite our prepared, Ag NPs just like the electron

transporter when the PDA act as the gripper which could grab methyl orange easily. Ag NPs transfer the electron to the surface of methyl orange to participate in the photocatalysis procedure. This process can be called collaborative operation. It makes photocatalytic reaction rapidly and thoroughly.

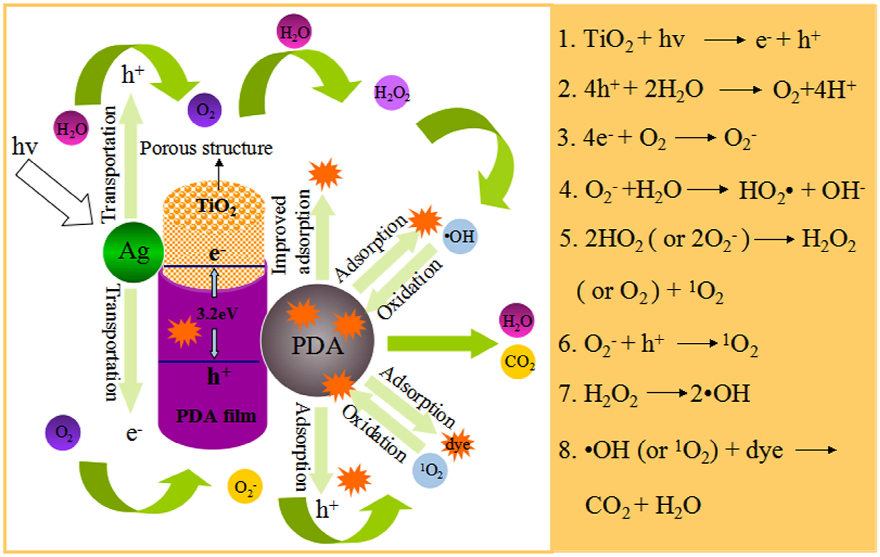

Fig. 8. Postulate mechanism for the photodegradation of methyl orange with the PDA-Ag/TiO2 porous NFs.

4. CONCLUSION

In summary, we have fabricated PDA-Ag/TiO_2 NFs composite by electrospinning technique and impregnation method. This composite just like a porous substrate embedded by the Ag NPs and wrapped by the PDA that we called it corn-like structure. The results of the photodegradation of methyl orange by ultraviolet light show that the corn-like PDA–Ag/TiO_2 NFs bionic composite catalyst exhibits high-efficiency photocatalytic activity. We could easily detect that the porous TiO_2 nanofibers fabricated by using the pore-forming of CNTs have higher specific surface area than pure TiO_2. This property make the TiO_2 NFs have the better adsorption performance which is beneficial to the photodegradation. In addition, Ag and PDA

can greatly improve the photocatalytic performance cooperatively. The synergistic effect between Ag and PDA is embodied in the process of photodegradation when PDA adsorb organic matter and the Ag NPs transport the electrons to the surface of PDA. Therefore, the PDA–Ag/TiO_2 porous NFs not only has the superior degradation property but also has the excellent adsorption capacity. This result indicates that PDA-Ag/TiO_2 NFs bionic composite catalyst could be applied in the field of adsorption degradation of organic pollutants.

Acknowledgments

The research is financially supported by the National Young Top Talents Plan of China (2013042), National Science Foundation of China (Grant No. 51175066), FANEDD (201164), New Century Excellent Talents in University (NCET-12-0704), and the Science Foundation for Distinguished Young Scholars of Heilongjiang Province (JC201403).

Reference

[1] M. R. Hoffmann, S. T. Martin, W. Choi and D. W. Bahnemann, *Chem. Rev*., 1995, 95, 69-96.

[2] X. C. Wang, J. C. Yu, Y. L. Chen, L. Wu and X. Z. Fu, Environ Sci Technol, 2006, 40, 2369-2374.

[3] M. Biancardo, P. F. H. Schwab, R. Argazzi, C. A. Bignozzi. *Inorg. Chem*., 2003, 42, 3966-3968

[4] S. H. Nam, H. S. Shim, Y. S. Kim, M. A. Dar, J. G. Kim and W. B. Kim, *ACS Appl. Mater. Interfaces*, 2010, 2, 2046-2052

[5] A. Pearson, H. Jani, K. K. Zadeh, S. K. Bhargava and V. Bansal, *Langmuir*, 2011, 27, 6661-6667.

[6] M. Jin, X. T. Zhang, S. Nishimoto, Z. Y. Liu, D. A. Tryk, A. V. Emeline, T. Murakami and A. Fujishima, *J. Phys. Chem. C*, 2007, 111, 658-665.

[7] X. W. Zhang, S.Y Xu, G. R. Han. *Mater. Lett.*, 2009, 63, 1761-1763.

[8] W. X. Dai, X. X. Wang, P. Liu, Y. M. Xu, G. S. Li and X. Z. Fu, *J. Phys. Chem. B*, 2006, 110, 13470-13476.

[9] P. Zhang, C. L. Shao, Z. Y. Zhang, M. Y. Zhang, J. B. Mu, Z. C. Guo and Y. C. Liu, *Nanoscale*, 2011, 3, 2943-2949.

[10] J. B. Mu, B. Chen, M. Y. Zhang, Z. C. Guo, P. Zhang, Z. Y. Zhang, Y. Y. Sun, C. L. Shao and Y. C. Liu, *ACS Appl. Mater. Interfaces*, 2012, 4, 424-430.

[11] P. D. Cozzoli, R. Comparelli, E. Fanizza, M. L. Curri, A. Agostiano and D. Laub, *J. Am. Chem. Soc*., 2004, 126, 3868-3879.

[12] S. Ko, C. K. Banerjee, J. Sankar. *Composites: Part B*, 2011, 42, 579-83.

[13] W. H. Zhou, S. F. Tang, Q. H. Yao, F. R. Chen, H. H. Yang and X. R. Wang, *Biosens. Bioelectron*, 2010, 26, 585-589.

[14] R. Liu, S.M. Mahurin, C. Li, R.R. Unocic, J.C. Idrobo, H. Gao, S. J. Pennycook and S. Dai, *Angew. Chem. Int. Ed*, 2011, 50, 6799-6802.

[15] J. Kong, W. A. Yee, L. Yang, Y. Wei, S. L. Phua, H. G. Ong, J. M. Ang, X. Li and X. Lu, *Chem. Commun*, 2012, 48, 10316-10318.

[16] M. Sureshkumar, P. N. Lee and C. K. Lee, *J. Mater. Chem*, 2011, 21, 12316-12320.

[17] Y. F. Li, S. F. Wang, H. Wu; J. T. Wang and Z. Y. Jiang, *J. Mater. Chem*. 2012, 22, 37, 19617-19620.

[18] L. Zhang, J. F. Shi, Z. Y. Jiang, Y. J. Jiang; R. J. Meng, Y. Y. Zhu; Y. P. Liang and Y. Zheng, *ACS Appl. Mater. Interface*, 2011, 3, 597-605.

[19] M. E. Lynge, R. V. Westen, A. Postmab and B. Städler, *Nanoscale*, 2011, 3, 4916-4928.

[20] N. M. Dimitrijevic, E. Rozhkova and T. Rajh, *J. Am. Chem. Soc*. 2009, 131, 2893-2899.

[21] W. Lee, J. U. Lee, B. M. Jung, J. H. Byun, J. W. Yi, S. B. Lee and B. S. Kim, *Carbon*, 2013, 65, 296-304.

[22] L. Q. Xu, W. J. Yang, K. G. Neoh, E. T. Kang and G. D. Fu, *Macromolecules*, 2010, 43, 8336-8339.

[23] H. Lee, B. P. Lee & B. Phillip. *Nature*, 2007, 448, 338-341.

[24] H. Lee, S. M. Dellatore, W. M. Miller, P. B. Messersmith. *Science*, 2007, 318, 426-430.

[26] N, Sobana, M, Muruganadham, M, Swaminathan, J Mol Catal A: Chem, 2006, 258:124–132.

[27] W. J. Wang, J. L. Zhang, F. Chen, D. N. He, A. Masakazu, J Colloid Interface Sci, 2008, 323:182–186.

[28] H. Y. Chuang, D. H. Chen, Nanotechnology, 2009, 20:105704–105713.